JOURNAL OF PROPULSION AND POWER
Vol. 20, No. 3, May–June 2004

Role of Radiation on Dynamic Extinction by Depressurization in Metalized Solid Propellants

Ho-Girl Jung,* Changjin Lee,† and Jae-Woo Lee‡
Konkuk University, Seoul 143-701, Republic of Korea

A numerical calculation was carried out to estimate and to elucidate the role of radiative heat flux from metal particles (Al and Al_2O_3) on dynamic extinction when rapid depressurization takes place. A one-dimensional unsteady energy equation for a condensed phase was solved with the quasi-steady gas-phase assumption. Also, nonlinear flame modeling for metalized propellant was adopted rather than direct numerical calculation with detailed chemical reactions. The decoupled radiative transfer equation was also solved for radiative heat feedback with use of a modified combustion-flow model. The calculation results with ammonium perchlorate: aluminum: carboxyle texminated polybutadiene (76:10:14) propellant revealed that the radiative heat flux is approximately 5–6% of the total heat flux at the critical depressurization. This 5–6% shows qualitatively good agreement in magnitude with experimental data of 2% of total heat flux. It was also found that the dynamic extinction in an open geometry could be predicted at about a 45% larger depressurization rate with radiative heat feedback than without radiation. Thus, it is concluded that even a small amount of radiative flux of 5–6% could produce a large error in predicting the critical depressurization rate of the metalized propellant combustion if not taken into consideration in the calculation.

Nomenclature

A	=	area
a	=	absorption coefficient
B_p	=	depressurization rate, $1.0 = 1.32$ atm/ms
c	=	specific heat
D	=	particle diameter
fv	=	volume fraction
E	=	activation energy
e	=	emission coefficient
I	=	radiative intensity
k	=	thermal conductivity
m_i'''	=	mass production rate of species i
P	=	pressure, atm
p	=	phase function
Q	=	heat release
q	=	radiative heat flux
R	=	nondimensional burning rate, $r_b/r_{b,\mathrm{ref}}$
R_u	=	universal gas constant
r_b	=	burning rate
s	=	scattering coefficient
T	=	temperature
t	=	time
t_g	=	residence time
t_{ref}	=	$\alpha_c/r_{b,\mathrm{ref}}$
U	=	velocity
V	=	combustor volume
x	=	space variable
$Y_{()}$	=	$T/T_{(),\mathrm{ref}}$
α	=	thermal diffusivity or absorptivity
γ	=	specific heat ratio
ε	=	emissivity
ε_r	=	fraction of q_0 absorbed in condensed phase
θ	=	$(T - T_{\mathrm{ref}})/(T_{s,\mathrm{ref}} - T_{\mathrm{ref}})$
ρ	=	density or reflectivity
τ	=	nondimensional time, t/t_{ref}
τ_g	=	nondimensional residence time, t_g/t_{ref}
ω	=	chemical reaction rate, 1/cm

Subscript and Superscripts

a	=	ambient condition
al	=	aluminum
b	=	burning or blackbody
c	=	condensed phase or chamber condition
f	=	flame or final
g	=	gas phase
i	=	initial state or species
ox	=	aluminum oxide
ref	=	reference state
s	=	surface
t	=	throat
0	=	the position at $x = 0$
$-$	=	steady state
$\pm$	=	forward/backward

Introduction

RAPID depressurization is one of the most effective ways to extinguish solid propellant combustion. When a solid rocket/booster has reached its ultimate velocity and/or altitude, controlled thrust termination is necessary for safe and successful system operation. A sudden increase of the nozzle throat area and/or opening of additional gas escape ports are commonly used methods in rocket systems. For example, the method with additional escape ports is adopted in the upper stages of Minuteman and Poseidon missiles. Thus, it is important to predict accurately the dynamic extinction of solid propellants for high performance and safe operation. The total heat flux to the solid fuel surface is shown to be the controlling factor in determining the characteristics of dynamic extinction behavior. If the depressurization rate is not sufficient and the resulting total heat flux is not suitably reduced to a critical value, then the surface temperature of the propellant tends to recover to a certain level sufficient to sustain combustion continuously following a short temporaty decrease, whereas if depressurization in the combustor is rapid enough to reduce the total heat flux to the

Received 23 October 2002; revision received 20 August 2003; accepted for publication 22 August 2003.

*Graduate student, Department of Aerospace Engineering.
†Professor, Department of Aerospace Engineering, Multidisciplinary Aerospace System Design Team; cjlee@konkuk.ac.kr.
‡Associate Professor, Department of Aerospace Engineering, Multidisciplinary Aerospace System Design Team.

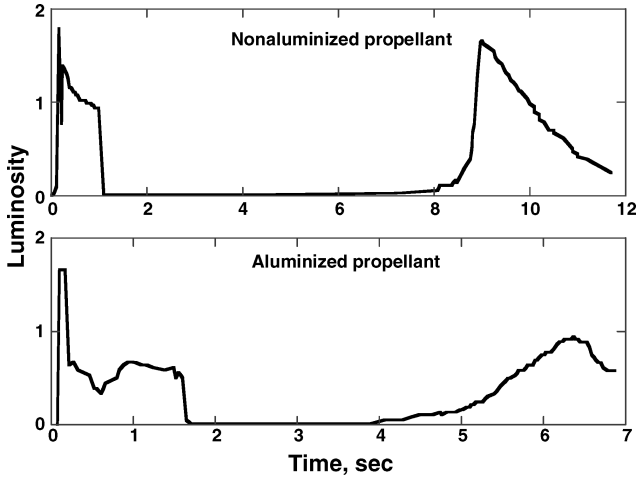

Fig. 1 Experimental results of spontaneous reignition of nonaluminized and aluminized propellants.[2]

solid fuel below a critical value, dynamic extinction of solid propellant conclusively occurs. Thus, examination of heat flux behavior on the fuel surface during depressurization is of vital importance in predicting the dynamic extinction of solid propellants. Note that the radiative heat flux is a significant fraction of the total heat flux in metalized solid propellant combustion.[1] Moreover, an experimental study by Ciepluch[2] showed different reignition behaviors between aluminized and nonaluminized propellants when the rapid depressurization was applied. His typical luminosity and pressure records showed that reignition of aluminized propellants occurred earlier than that of nonaluminized propellants because of an additional radiative heat flux from metal particles. Figure. 1 is a redrawn schematic of the luminosity records of both propellants. Thus, the radiative heat flux may be crucial in determining the dynamic extinction behavior of aluminized propellants.

In addition, note that aluminum is a common ingredient frequently used for the suppression of combustion instabilities and the increase of specific impulse in composite/composite modified double base (CMDB) solid propellants. It is also well known that Al and Al_2O_3particles in the combustor behave as the major radiation sources until they flow out through the nozzle. Therefore, the analysis of dynamic extinction of metalized propellants cannot be completed without having the estimation of radiative heat flux to the solid fuel surface from Al and Al_2O_3particles. Unfortunately, however, details of Al combustion in the gas region are still not completely understood, and no relevant modeling of Al combustion is available for numerical calculation coupled with gas-phase chemical reaction.

Many studies extensively pursued this subject following the pioneering works by Ciepluch,[3] Krier et al.,[4] and Kuo et al.[5] Merkle et al.[6] proposed a convenient way to calculate the conductive heat flux without resorting to the detailed reaction kinetics, rather using the phenomenological flame model that was associated with the residence time modeling of the mixture in the gas region. De Luca[7] adopted the $\alpha\beta\gamma$ model, a more advanced flame model than that of Merkle et al.[6] Galfetti et al.[8] did numerical studies of the intrinsic instabilities in the solid propellant combustion, as well as the dynamic extinction. Meanwhile, Brewster and Perry[1] estimated the amount of radiative heat flux in the steady combustion of metalized solid propellants by using the combustion-flow model in which the simple reaction of an Al particle in the gas phase was accounted for. Ishihara et al.[9] conducted experiments to measure the radiative heat flux in steady combustion of Al composition propellant of 0–20%.

Despite significant progress, in the study of metalized propellant combustion, it is not easy to find any attempts to identify the role of radiative heat flux on dynamic extinction in rapidly depressurized combustor, which is the motivation for this study. Numerical calculation had been carried out to estimate the amount of radiative heat flux and to identify the role of radiative flux on the behavior of dynamic extinction of metalized solid propellant combustion.

Formulation and Modeling

The estimation of the radiative heat flux in rapidly depressurized combustion requires simultaneously solving a few coupled governing equations: the unsteady energy equation for both the condensed phase and gas phase and the two-phase radiative transfer equation in the participating medium coupled with gas-phase energy equation. It is so complex and formidable that the numerical calculation with detailed chemistry is not easy even in one-dimensional simple geometry. Moreover, the combustion process of Al is still not completely known to scientists. Hence, the proper formulation and the plausible assumptions should be made to obtain a qualitative estimation of the radiative heat flux and to facilitate the complexity of the calculation.

In this study, some assumptions and modelings are implemented in the problem formulation for a simple and qualitative analysis. One of them is the quasi-steady assumption in the gas phase. In solid propellant combustion, it is quite possible to that consider that the gas phase adjusts to the external disturbances much faster than the condensed phase, which makes the otherwise fully unsteady burning transient a quasi-steady gas-phase burning. The nonlinear flame modeling, known as the $\alpha\beta\gamma$ model, was used to describe qualitatively the heat release distribution by the use of experimental data. Because the flame model essentially accommodates the different propellant flames, careful adjustments of the heat release distribution and validity checks by comparison with experimental data are necessary to obtain meaningful results in the calculation.

In addition, the radiative transfer equation in the participating medium was decoupled from the gas-phase temperature profile.[10] The details of the formulation will be discussed in each subsection. Note that the agglomeration is of importance in determining the overall combustion behavior and radiation heat transfer. However, the effect of the agglomeration of Al combustion was not taken into account for the simple analysis.

Governing Equation in Condensed Phase

Consider a semi-infinite propellant slab of uniform composition with 10% of Al particles as shown in Fig. 2. The aluminized solid fuel is assumed to move in the positive x direction, and the origin of the axis coincides with the surface. The radiative heat flux is accounted for by the use of fraction parameter ε_r in the governing equation. Then the unsteady energy equation is expressed as

$$\rho_c c_c \left(\frac{\partial T}{\partial t} + r_b \frac{\partial T}{\partial x} \right) = k_c \frac{\partial^2 T}{\partial x^2} + \varepsilon_r q_0 a_c e^{a_c x} \tag{1}$$

where ρ_c, c_c, and k_c are assumed constant and q_0 is the radiative heat flux from the cloud of metal particles in the gas phase. The pyrolysis burning surface is infinitesimally thin and subject to a one-step irreversible gasification process that can be expressed by the classical Arrehnius formula $r_b = A \exp(-E_s/R_u T_s)$. The radiative heat flux is formulated based on Beer's law. Only a fraction ε_r of the radiative flux on the surface is assumed to be absorbed in the condensed phase, whereas the remainder $(1 - \varepsilon_r)$ is absorbed in the thin reaction zone. Boundary and initial conditions

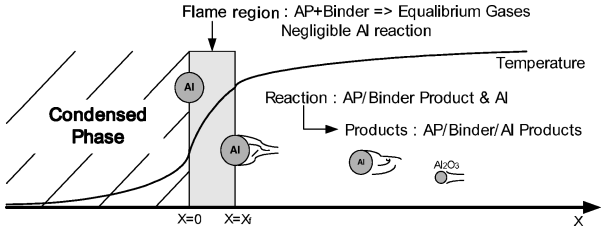

Fig. 2 Schematic of combustion of condensed and gas phases in metalized solid propellants.

are following

$$T(x \to -\infty, t) = T_a \tag{2a}$$

$$\left(k_c \frac{\partial T}{\partial x}\right)_{0^-} = \left(k_g \frac{\partial T}{\partial x}\right)_{0^+} + \rho_c r_b Q_s + (1-\varepsilon_r) q_0 \tag{2b}$$

$$T(x, t=0) = T_i \tag{2c}$$

The fraction parameter ε_r (Ref. 11) represents the transmissivity of the radiation through the reaction zone and is defined as

$$\varepsilon_r = \exp\left(-\frac{a_c \alpha_c / \bar{r}_b}{E_c / 2R\bar{T}_s}\right) \tag{3}$$

No reflection on the surface was taken into account in the calculation. The first term in boundary condition (2b) is the conductive heat flux to the condensed phase, and the second term should be evaluated by the gas-phase energy equation. Thus, it is obvious that the condensed-phase energy equation is strongly coupled with the gas-phase energy equation. The radiative heat flux q_0 is also needed to solve the energy equation in the gas phase and can be obtained from the radiative transfer equation.

Modeling in Gas Phase

It is assumed that the gas-phase region consists of two subregions: the flame region and the Al burning region. The former is a relatively thin region compared to the initial Al diameter near the propellant surface, where the most chemical reaction of ammonium perchlorate (AP)/binder takes place. The latter, however, remainder of the gas region, and the radiation from Al and Al_2O_3particles dominates.

Nonlinear Flame Modeling

The chemical reaction in the region is quite complex, so that it is not easy to include every chemical reaction step and species in the calculation. Thus, not surprisingly a less complex method is used to calculate the temperature distribution and the heat conduction from the gas phase, without resorting to detailed chemistry. The nonlinear $\alpha\beta\gamma$ flame model is one of the methods used for this purpose. Many models have been proposed, and the validity of this model has been proven in previous studies.[6–8] The energy equation in the gas phase with a quasi-steady assumption can be written

$$\rho_g c_g u_g \frac{\partial T}{\partial x} = k_g \frac{\partial^2 T}{\partial x^2} + \rho_g Q_g \omega \tag{4}$$

This equation is only valid in the region $0 \le x \le x_f$, where the most AP/binder reaction occurs. Here, the thickness of flame region x_f is so small compared to the initial Al size that the chemical reaction of Al was considered negligible in this region. Then it is not difficult to deduce the conductive heat flux to the propellant surface by simply integrating the energy equation in the range of $0 \le x \le x_f$. The heat conduction becomes

$$k_g \left(\frac{\partial T}{\partial x}\right)_{0+} = \int_{0^+}^{x_f} \rho_g Q_g \omega \exp\left(-\frac{c_g}{k_g} \rho_c r_b x\right) \mathrm{d}x \tag{5}$$

Detailed derivations may be found in Ref. 7.

The formal integration of Eq. (5) requires two separate modelings: the heat release distribution and the thickness of flame region x_f, which can be determined by the residence time modeling. The parameters α, β, and γ could decide the heat-release distribution in the flame region and should properly represent the overall heat-release distribution in the flame region. Details of the modeling may be found in Ref. 7. Measured profiles of volumetric heat-release rate of aluminized composite propellants are found in Ref. 12. The parameters of α, β, and γ were selected as $\alpha = 0.2$, $\beta = 0.9$, and $\gamma = 1.0$ to match the qualitative description of volumetric heat-release rate. Once x_f is determined, then the chemical reaction rate could be evaluated. Because the residence time t_g of the mixture in the gas region depends on the thermodynamic state, such as the surface temperature and the pressure, it is appropriate to express the residence time t_g as a product of two separate functions of $f(P)g(r_b)$ (Ref. 7). Here, $f(P)$ is an arbitrary function of pressure and $g(r_b)$ the dependency on the burning rate. Function $f(P)$ can be easily evaluated under the steady-state condition and is valid in the quasi-steady condition as well. Physically, the residence time is approximately a sum of various contributions such as diffusion time, chemical reaction time, evaporation time, etc. Merkle et al.[6] suggested a few residence time models using the various combinations between diffusion and kinetic times for nonmetalized AP-based composite propellants. Although there are a few flame models relevant to nonmetalized propellants, no flame models have been publicly reported for metalized propellants. Thus, $g(r_b)$ should be properly modeled and checked against experimental data. In this study, various combinations of $g(r_b)$, along with the diffusion and kinetic timescales, were examined and compared with the experimental data. It is well known that the nondimensional diffusion g_1 and the kinetic g_2 time are proportional to following relations, respectively[7]:

$$g_1 = Y_f^2 \exp[(E_g/R_u T_f)(1/Y_s - 1)] \qquad g_2 = Y_f^{\frac{5}{3}} \Big/ Y_s^{\frac{7}{4}} \tag{6}$$

Validation of Nonlinear Flame Modeling

To check the validity of the flame modeling, a nonmetalized propellant, AP/hydroxyl terminated polybutadiene (HTPB) = 86:14, was selected. Figure 3 shows the calculation results of surface temperature to choose the appropriate residence time modeling. The calculated results were compared with previous data of Ref. 8. Five combinations of nondimensional residence time τ_g were used to determine the proper function of g: case 1, $f(P)(g_1^{1/2} + g_2^{1/2})/2$ case 2, $f(P)(1/g_1 + 1/g_2)/2$; case 3, $f(P)\,\lfloor (1/g_1)^{1/2} + (1/g_2)^{1/2} \rfloor/2$; case 4, $f(P)(g_1 + 1/g_2)/2$; and case 5, $f(P)(1/g_1 + g_2)/2$. As can be seen in Fig. 3, case 5 yields quite good agreement with previously measured data. Thus, case 5 was selected for the flame modeling in the rest of calculations.

Ishihara et al.[9] measured experimentally the radiative heat flux and the conductive heat flux to find the influence of the variation of Al concentration on the propellant combustion. The results show that the conductive heat flux to the propellant surface depends only on the chamber pressure, and the variation of Al concentration from 0 to 20% does not significantly alter the conduction level. Thus, it is possible to assume that the conductive heat flux is independent of Al concentration.

The conductive heat flux was also calculated with the flame modeling implemented by the residence time function of case 5 for a metalized propellant of composition AP/Al/carboxyl terminated polybutadiexe (CTPB) = 76:10:14. The calculation result is shown in Fig. 4. Comparison is made between the present calculation and the experimentally obtained data[9] for the propellant having the same Al concentration. As shown in Fig. 4, the calculation result can produce fairly good agreement in conductive heat flux with experimental

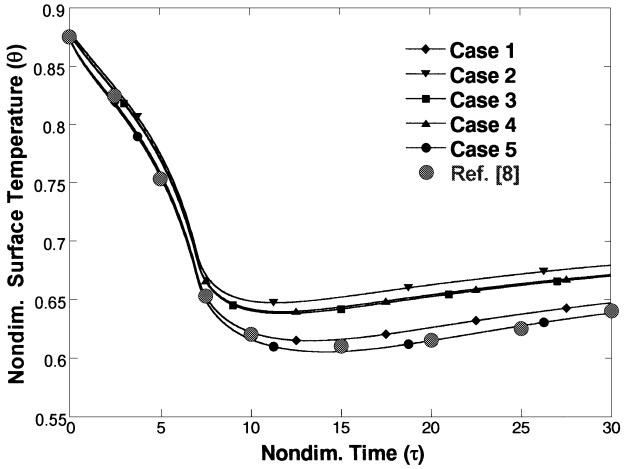

Fig. 3 Verification of residence time modelings used in the flame model with nonmetalized propellant.

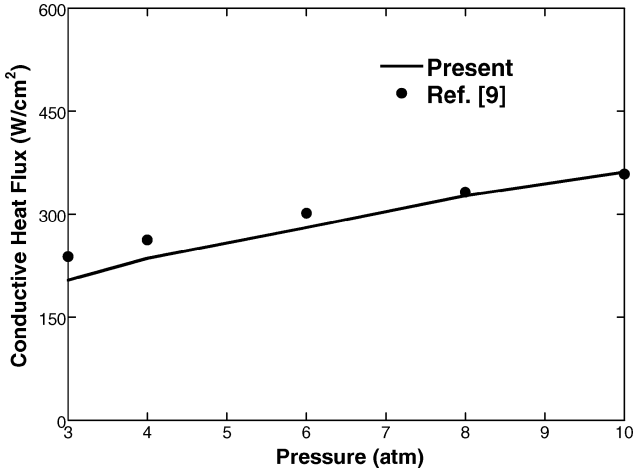

Fig. 4 Comparison of current conductive heat flux with that obtained by the measurement in Ref. 9.

data. Therefore, the present flame model was implemented by the case 5 residence time function. Although this model was verified with propellant of 0% Al composition, it can be applied to Al propellants. Also note that the case 5 combination for residence time can be qualitatively extended to the function of metalized propellants, although its validity was checked with only nonmetalized propellants.

Rapid Depressurization in the Combustor

The numerical calculation was carried out with two types of combustor geometry: open combustor and confined combustor. Dynamic extinction is the manifestation of intrinsic combustion instability of the solid propellant. Thus, many factors could influence the characteristics of dynamic extinction. In this study, two cases of combustion chamber geometries are considered in the calculation: open and confined geometry. Open geometry represents the combustion condition in an unconfined vessel. Therefore, the pressure decreases and remains constant in this case. The pressure is not coupled with the combustion, but is provided as an input value. In actual operation, the sudden increase in nozzle throat area can lead to the of chamber pressure coupling with propellant combustion. The pressure is determined by the consideration of mass generation and depletion. The combustion, however, could be influenced by the depressurization rate only in an open combustor, whereas the pressure coupling effect can be seen in a confined combustor attached with choked nozzle.

In an open geometry, chamber pressure can be linearly decreased from initial pressure P_i to final pressure P_f with arbitrary depressurization rate B_p and then remains at P_f thereafter. The equation of pressure change during depressurization is expressed as $P(t) = P_i - B_p \cdot t$. However, in a confined geometry, the pressure followed by the linear depressurization period is determined by considering the balance between mass production and depletion through the choked nozzle. The following equation shows the mass balance in the combustor.

$$A_b \rho_c r_b = \frac{\mathrm{d}}{\mathrm{d}t}(\rho_c V_c) + \frac{A_t P_c}{\sqrt{T_f (R_u/\mathrm{MW})}}\,\Gamma \tag{7}$$

where

$$\Gamma = \sqrt{\gamma [2/(\gamma+1)]^{(\gamma+1)/(\gamma-1)}} \tag{8}$$

The average molecular weight (MW) of gases was assumed 28 g/mole in the calculation. If the changes of chamber volume V_c and flame temperature T_f are negligibly small, then Eq. (7) becomes a function of P_c as

$$P_c(t) = \frac{\sqrt{T_f R_u/\mathrm{MW}}}{\Gamma A_t}\left(A_b \rho_c r_b - \frac{V_c}{T_f}\frac{\mathrm{MW}}{\mathrm{R_u}}\frac{\mathrm{d}P_c}{\mathrm{d}t}\right) \tag{9}$$

Thus, the chamber pressure P_c is determined in the calculation.

Al Combustion and Radiation

Both gas and metal particles (Al and Al_2O_3) may contribute to radiative heat transfer in combustion. Generally, soots and infrared emitting gases are the primary sources of radiation in nonmetalized propellant combustion. For metalized propellants, however, the cloud of Al and Al_2O_3 particles is the main source of radiation in the gas phase, and the contribution of gases and soots are assumed negligibly small in the analysis. Thus, the focus was put on the radiative heat flux from the cloud of Al and Al_2O_3 particles only. Also, although the agglomeration of Al droplet size is of importance in the analysis of the radiation of aluminized propellant combustion, only the experimental correlation was used to account for the initial agglomeration of Al diameter. Nickerson et al.[13] suggested a correlation between the initial diameter and the chamber pressure based on the experimental data. According to the correlation, the calculated initial Al diameter at 1 atm was on the order of 1000 μm in this study, which is somewhat exaggerated and physically unacceptable. Because to the author's knowledge, there are no available references on this matter the maximum initial Al diameter was assumed not to exceed 500 μm during depressurization in the calculation.

Moreover, although it is true that Al and Al_2O_3 particles respond in a transient manner to the pressure change, the adjustment time of particles to the perturbations was assumed to be the same order as that of the gas phase and the quasi steady state consequently could be valid.

The radiative transfer equation was solved by the two-flux method in the semi-infinite slab geometry. Then the radiant transfer equation is

$$\frac{\mathrm{d}I}{\mathrm{d}x} + (a+s)I = eI_b + \frac{s}{4\pi}\int_{4\pi} I(x)\,p(\Omega', \Omega)\,\mathrm{d}\Omega' \tag{10}$$

The boundary conditions are

$$\left.\frac{\mathrm{d}I^+}{\mathrm{d}x}\right|_{\infty} = 0, \qquad I^+(0) = 0 \tag{11}$$

Heat flux $q_0 = \pi \mathrm{I}^-$ is a radiative feedback to the burning surface, and p is a phase function for scattering. I^+ is the radiation intensity to the positive x direction away from the surface, and I^- is irradiation. Note that the surface reflection was neglected, and the surface emission was not accounted for either. All of the radiation coefficients a, s, and e for spherical particles can be expressed by a function of volume fraction and the particle diameter. To obtain the function, we adopted the combustion-flow model proposed by Brewster and Parry.[1] The diameter of Al_2O_3 particles is practically a function of spatial position. However, the particle diameter is assumed to be a constant 0.3μm in the entire gas region and to have a mono-dispersion characteristic. The optical properties of Al and Al_2O_3 excerpted from Ref. 1 are $\alpha = 0.1$, $\rho = 0.9$, and $\varepsilon = 1.0$ for Al and $\alpha = 0.65$, $\rho = 0.35$, and $\varepsilon = 0.3$ for Al_2O_3.

Basically the gas phase consists of two phases: the gas phase and the particle cloud of Al. Thus, it is necessary to have equations for two-phase quasi-steady momentum and for species conservation. For Al particles, the momentum equation is

$$\rho_{\mathrm{al}(l)}\left[U_{\mathrm{al}}\frac{\partial U_{\mathrm{al}}}{\partial x}\right] = 3\rho_g (U_g - U_{\mathrm{al}})\,|U_g - U_{\mathrm{al}}|\frac{C_d}{4D_{\mathrm{al}}} \tag{12}$$

The momentum equation for the gas phase is

$$\rho_{g0} f v_{g0}\left[U_g \frac{\partial U_g}{\partial x}\right] = (U_g - U_{\mathrm{al}}) m'''_{\mathrm{al}(l)}$$

$$- 3\rho_g f v_{\mathrm{al}(l)} (U_g - U_{\mathrm{al}})\,|U_g - U_{\mathrm{al}}|\frac{C_d}{4D_{\mathrm{al}}} \tag{13}$$

It is assumed that the temperature of Al is expressible as a simple function of pressure (atmospheres) (Ref. 1) as

$$T_{\mathrm{al}} = 393.3\,\ell_n(10^{-5}P) - 2273 \tag{14}$$

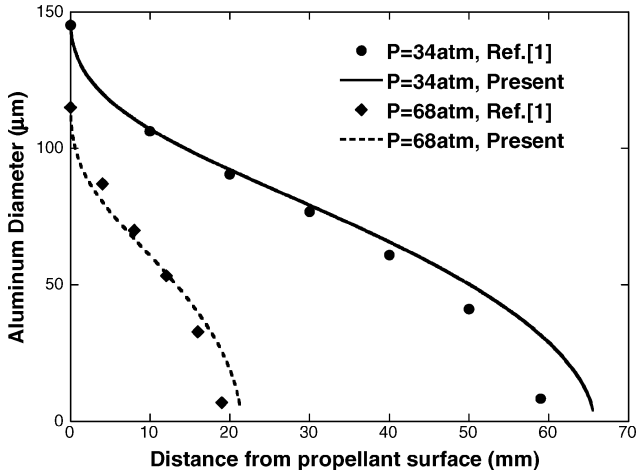

Fig. 5 Comparison of Al diameter distribution of present study with previous results[1] at steady state.

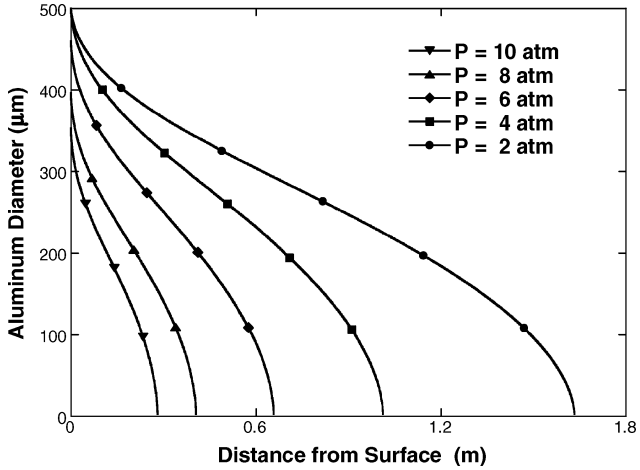

Fig. 6 Spatial distribution of Al diameter at various pressures with a reduced number of species.

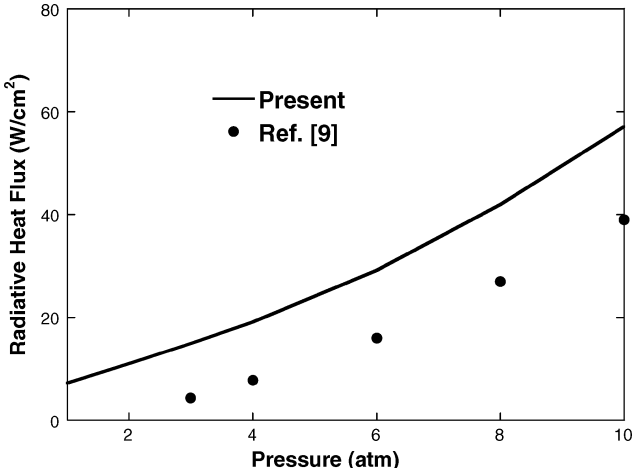

Fig. 7 Comparison of current radiative heat flux with that in Ref. 9.

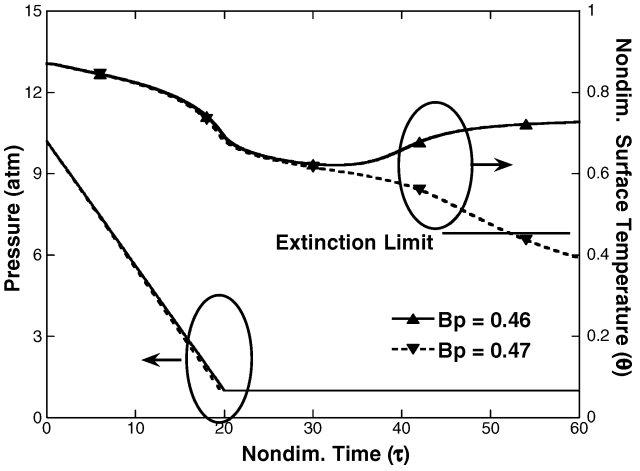

Fig. 8 Dynamic extinction in rapid depressurization without radiation in open geometry.

The species conservation equation has the form

$$\frac{\partial\left(\rho_i f v_i U_i\right)}{\partial x} = m_i''' \tag{15}$$

Although there is a new experimental result for the diameter for single and agglomerated Al droplets,[14] the classical D^2 law of Nickerson et al.[13] was used to calculate Al production rate. The initial diameter of the Al particle becomes

$$\frac{\mathrm{D_{al}}}{\mathrm{D_{0,al}}} = \left(1 - \frac{kt}{\mathrm{D_{al}}}\right)^{1/1.8}, \qquad \frac{\mathrm{D_{0,al}} = 1}{(1.1248 r_b f m_{\mathrm{AP}})} \tag{16}$$

Details of the where burning rate r_b is in meters per second. combustion-flow model may be found in Ref. 1. In the chemical reaction, only a reduced number of species of H_2, CO_2, H_2O, HCl, N_2, Al, and Al_2O_3 was considered to minimize calculation time without loss of accuracy. Figure 5 shows the calculated Al diameter spatial distribution result compared to that of Ref. 1 for the gas region. As Fig. 5 shows, the distribution of Al diameter is in good agreement with the previous calculation. At 34 atm, Al particles could be burned out at the location of 6.5 cm farther than that of the 2.2 cm at 68 atm. Figure 6 shows the calculation result of the distribution of Al diameter at each pressure. The lower the chamber pressure is, the larger is the Al diameter at the propellant surface and the broader is the distributed region of Al. In Fig. 7, it can be seen that, with proper modelings, the calculation predicts the radiative flux with good accuracy. The discrepancy between the calculation and experiment seems mainly due to the Al agglomeration being ignored.

By the use of this modeling, numerical calculations are conducted with an aluminized propellant of AP:Al:CTPB = 76:10:14. This propellant is not a specific one, but a commonly available propellant. Material properties are mainly excerpted from Refs. 15 and 16 and are as follows: $\rho_c = 1.678$ g/cm^3, $c_c = 0.37$ cal/g·K, $k_c = 0.0004$ cal/cm·s·K, $\bar{T}_s = T_{s,\mathrm{ref}}\ (P/P_{\mathrm{ref}})^{0.051}$K, $\bar{T}_f = T_{f,\mathrm{ref}}\ (P/P_{\mathrm{ref}})^{0.1}$K, $\bar{Q}_s = 85\ (P/P_{\mathrm{ref}})^{0.049}$ cal/g, $E_s = 17,500$ cal/mol, $P_{\mathrm{ref}} = 68$ atm, $T_{s,\mathrm{ref}} = 964.8$ K, $T_{f,\mathrm{ref}} = 2384$ K, and $T_{\mathrm{ref}} = 300$ K.

Results and Discussion

Figure 8 shows the result of dynamic extinction of the solid propellant with rapid depressurization from $P_i = 10.2$ atm to $P_f = 1$ atm in an open combustor. Here, the depressurization rate B_p is an input parameter and can be changed until dynamic extinction occurs. This calculation result merely shows a duplication of the well-known result found in Ref. 8. The radiative heat flux was not included. As can be seen, the surface temperature recovers to a steady value only after a short-period temperature drop when the depressurization rate B_p is 0.46.

However, the temperature trace shows a monotonic decrease and leads to permanent extinction when B_p is 0.47. This is the onset of solid propellant combustion dynamic extinction with rapid depressurization, Thus, $B_p = 0.47$ can be regarded as the critical depressurization rate below which dynamic extinction always occurs for a given propellant. Note that the temperature limit for the extinction was defined as 600 K surface temperature, which is the same criterion as in Ref. 6.

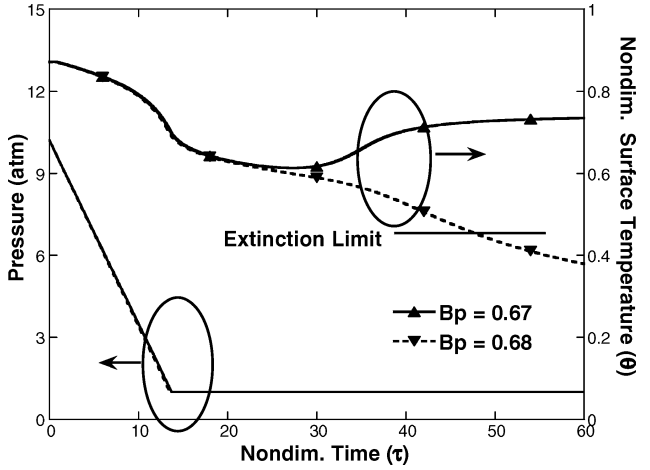

Fig. 9 Dynamic extinction with radiation in open geometry.

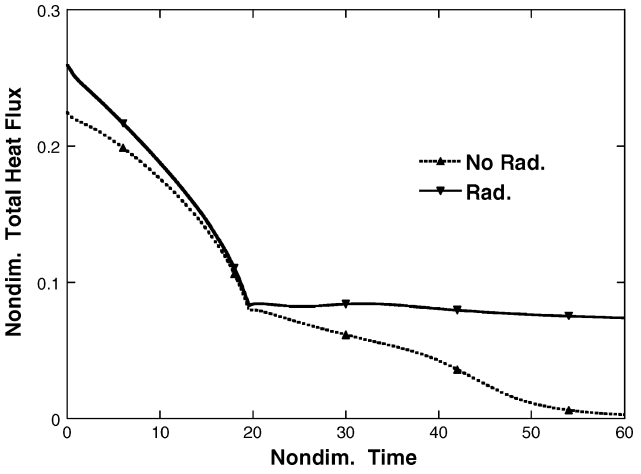

Fig. 10 Comparison of total heat flux transitions with/without radiation at $B_p = 0.47$.

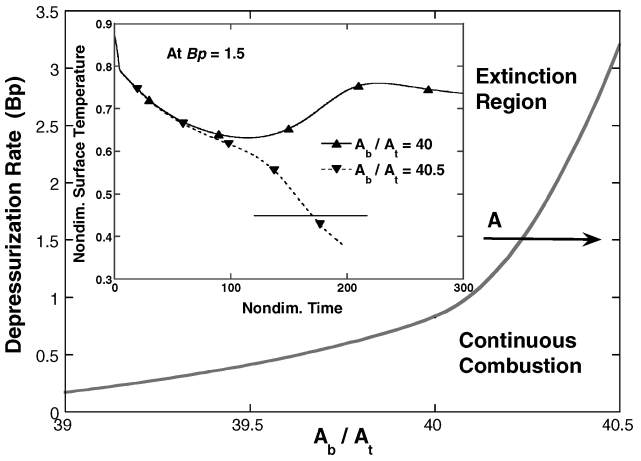

Fig. 11 Relationship A_b/A_t with critical B_p in confined geometry at $P_f = 4.0$ and $L^* = 350$.

Dynamic extinction, however, occurs at a different depressurization rate when the radiative heat flux is accounted for in the calculation. Figure 9 shows trajectories of pressure and the surface temperature when the depressurization was applied in the combustion. Here, the critical depressurization rate B_p is 0.68, and it is about 45% larger than that calculated without radiative heat flux. It is not surprising that the combustion becomes more robust against depressurization if an additional radiative heat flux to the solid fuel surface exists. For the extinction time, the calculation showed that dynamic extinction occurs at $\tau = 48$, as shown in Fig. 9. However, Fig. 8 shows that extinction takes place a little earlier than $\tau = 51$ obtained without radiation. Thus, we find that the prediction of dynamic extinction of the metalized propellant combustion in open geometry is quite dependent on the existence of radiative heat flux, even when the magnitude of the radiative flux is about 5–6% of the total flux to the propellant surface, and this will be shown later.

In addition, note that surface temperature trajectories in Figs. 8 and 9 have two different negative slopes during the initial depressurization period. The surface temperature decreases with a relatively smaller negative slope until 5-atm pressure, followed by the abrupt change in pressure drop. This is due to the difference in the timescales between the depressurization time and the response time of the condensed phase. It is instructive to estimate the response timescale (α_c/r_b^2) of the condensed phase and the characteristic depressurization timescale $[|\Delta P|/(\mathrm{d}P/\mathrm{d}t)]$. The response time of the condensed phase is calculated as about 2.6×10^{-4} s in this study, and this is comparable in magnitude to the time lapse of depressurization from 10 to 5 atm (5.7×10^{-4} s). The condensed phase needs an initial time delay to react to the pressure perturbations for the condensed phase to catch up with the gas phase because of a large thermal inertia of the propellant compared to that of gas phase. Then the condensed phase reacts synchronously to the perturbations by showing a larger negative slope.

Figure 10 shows the comparison of total heat flux transitions at the propellant surface for two cases. A solid line represents the transition of heat flux calculated with radiative heat flux at the critical depressurization rate of $B_p = 0.47$, whereas a dotted line indicates a history of the total heat flux obtained without accounting for radiation. As expected, radiative heat flux can provide an additional flux during the depressurization, as well as keep the total heat flux nearly constant, as indicated in Fig. 10 with the solid line. Consequently, this additional heat flux causes spontaneously reignition. However, combustion recovery is not possible if the radiation is neglected. The transition of heat flux shows a continuous drop and results in the permanent extinction with the depressurization.

In the confined geometry, dynamic extinction shows a complicated dependency on many parameters such as burning area A_b, throat area A_t, combustion chamber volume V_c, final pressure P_f, and depressurization rate B_p. In the calculation, however, there are four parameters involved: area ratio A_b/A_t, characteristic length $L^* = V_c/A_t$, final pressure P_f, and depressurization rate B_p. Note that the initial pressure P_i is fixed as 10.2 atm for all cases in the calculation. Figures 11–14 show the calculation results, demonstrating the effect of each parameter on dynamic extinction. Although direct comparison of calculation results for the two types of geometry is not possible, the overall behavior of dynamic extinction in confined geometry shows qualitatively the same behavior as that observed in the open geometry. The calculation results indicate that it takes a slightly longer time for the combustion in the confined geometry to be extinguished. For example, dynamic extinction in the open geometry occurs at about $\tau = 50$. However, the calculation for the confined geometry shows that the extinction time is on the order of 200, as shown in Figs. 11–14. The confinement effect resulting in the pressure recovery is the physical reason attributed to the lengthening of the extinction time.

The effect of burning area A_b/A_t on dynamic extinction is shown in Fig. 11. Dynamic extinction occurs at $A_b/A_t = 40$ with other parameters fixed, $L^* = 350$, $P_f = 4.0$ atm, and $B_p = 1.5$. Also, it is not difficult to find that the larger the burning area (A_b/A_t increases), the steeper is the depressurization rate required for extinction. Physically, the larger burning area means more gas generation in the combustor. Thus, larger gas depletion is required to cause complete extinction. Figure 12 shows a calculation result similar to that shown in Fig. 11. Figure 12 shows final pressure P_f against B_p with fixed characteristic length L^* of 350 and area ratio A_b/A_t of 40. As the final pressure P_f increases, it is not easy for dynamic extinction to take place. With depressurization rate $B_p = 0.5$, extinction occurs

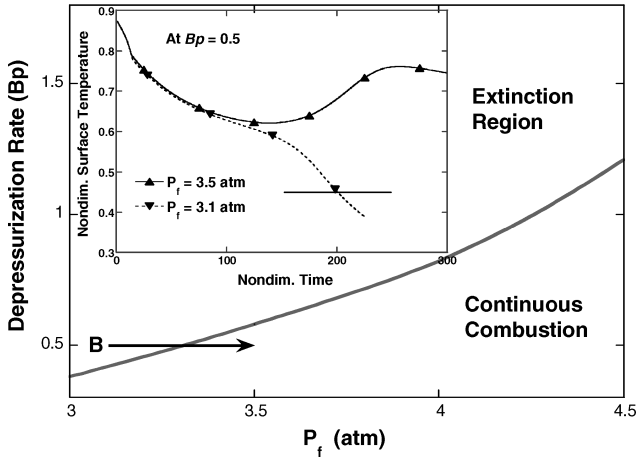

Fig. 12 Relationship P_f with critical B_p in confined geometry at $A_b/A_t = 40$ and $L^* = 350$.

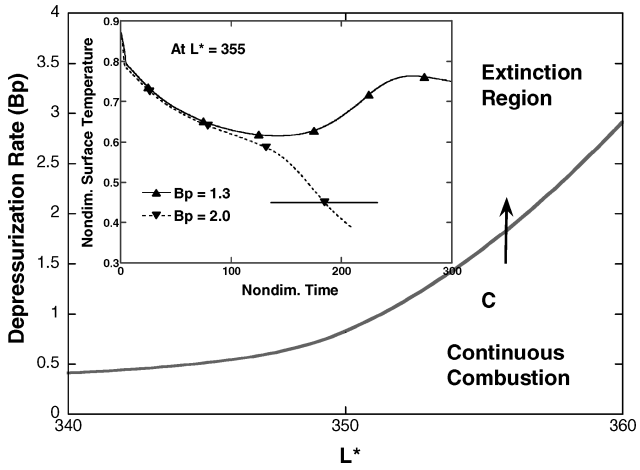

Fig. 13 Relationship L^* with critical B_p in confined geometry at $A_b/A_t = 40$ and $P_f = 4.0$.

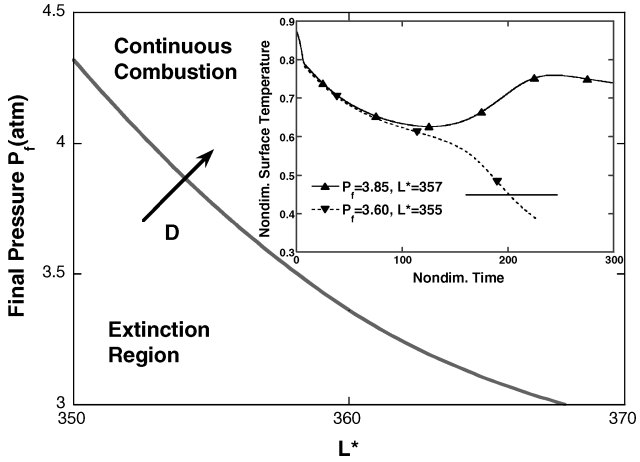

Fig. 14 Relationship L^* with P_f at $B_p = 1.0$ and $A_b/A_t = 40$.

at $P_f = 3.1$ atm, but it does not take place at the final pressure $P_f = 3.5$ atm. Also, it is found that the higher the final pressure P_f, the larger the critical depressurization rate for dynamic extinction needs to be. The effect of chamber volume with L^* was investigated, and the results are shown in Fig. 13. Similar to other cases, the larger the characteristic length L^*, the larger B_p needs to be for extinction. Figure 14 shows the effect of L^* and P_f on dynamic extinction when $B_p = 1.0$ and $A_b/A_t = 40$. As shown in Fig. 14, dynamic extinction

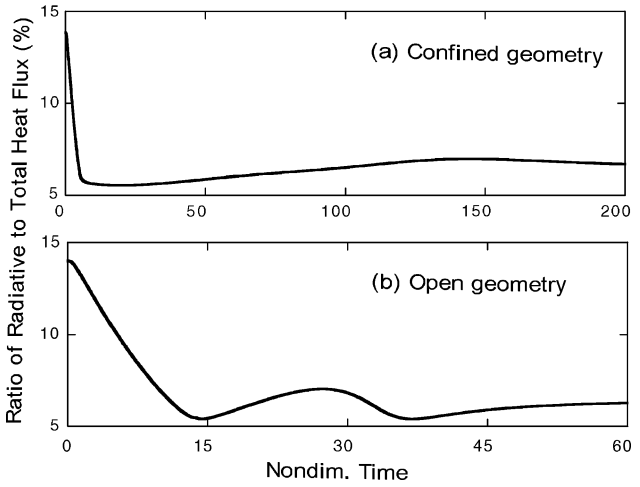

Fig. 15 Fraction of radiative heat flux of total heat flux with a) $B_p = 1.5$, $A_b/A_t = 45$, $P_f = 2.5$ atm, and $L^* = 350$ and b) $B_p = 0.67$.

with larger L^* (larger combustor volume) does not occur easily if final pressure P_f is not sufficiently small.

When the burning area $A_b/A_t = 44$, final pressure $P_f = 3.3$ atm, and $L^* = 352$, the critical depressurization rate B_p is calculated to be 0.9, if the radiation is excluded from the calculation. However, the critical depressurization rate becomes 6.6 if the radiation is accounted for when burning area $A_b/A_t = 43$, the final pressure $P_f = 3.3$ atm, and $L^* = 352$. The depressurization rate B_p with radiation is found to be approximately seven times larger than that obtained without radiation in the confined geometry. However, the effect of radiative heat flux shows an increase of B_p by only 45% in the open geometry. Thus, it is demonstrated that radiation takes a more important role in determining the behavior of dynamic extinction in the confined geometry than in the open geometry.

Meanwhile, it is quite important, to estimate the fraction of radiative heat flux at the critical depressurization rate in both the open and the confined geometry. Figure 15 shows the trace of the fraction of radiative flux on the propellant surface during the depressurization. When the pressure decreased rapidly from P_i to P_f, the fraction of radiative flux starts to decrease from about 14% to $5-6$%. Ishihara[9] measured the fraction of radiative heat flux at various steady-pressure levels with metalized propellants using fiber optics. Their results show that radiation comprises about 10% of total incident heat flux to the propellant surface at 10 atm when the propellant has 10% Al. Also, the fraction of radiation was shown to be about 2% at the combustion pressure of 2 atm.

Here, note that the propellant composition used in the experiment was AP/Al/HTPB = 73.8 : 10 : 16.2. This propellant has different composition from the propellant AP/Al/CTPB = 76 : 10 : 14 adopted in the current calculation. Despite the difference in propellant compositions, the calculated fraction of radiative heat flux at 10 atm shows qualitative good agreement with the experimental data. Also, note that the fraction of radiative flux of 2% at pressure of 2 atm in the experiment is comparable with the calculated result of 5–6% in total heat flux. It is, therefore, plausible that the modeling and assumptions in this study can be regarded as appropriate and that the calculation result shows qualitative good agreement with the experimental data.

Also, the radiative heat flux is of vital importance in predicting dynamic extinction of metalized solid propellants. Even a small amount of radiative heat flux (5–6% of total flux) can cause an error of about 45% larger value in the critical depressurization rate.

Conclusions

The numerical calculation had been carried out to estimate the amount of radiative heat flux and to identify the role of radiative flux in the behavior of dynamic extinction of metalized solid propellant combustion. Also, the effect of radiative heat flux on dynamic extinction was investigated both in open and confined geometry. The

calculation was done with appropriate modelings, rather than with direct numerical calculation with detailed chemical kinetics. The decoupled radiative transfer equation was also solved to obtain the radiative heat feedback with the aid of a modified combustion-flow model. In the combustion-flow model, the distribution of particle diameters and the particle volume fractions were properly calculated, and the radiation coefficients were evaluated, which is necessary for the calculation of radiation intensity in the participating medium.

The calculation results with the propellant of AP:Al:CTPB = 76 : 10 : 14 revealed that the radiative heat flux is approximately 5–6% of total flux at the critical depressurization rate regardless of chamber geometry (open or confined chamber). This of 5–6% of radiation shows qualitative good agreement in magnitude with the experimentally measured radiative flux of 2% of total flux. Also, it was found that dynamic extinction in the open geometry could be predicted at the depressurization rate of about 45% larger with radiative heat feedback included in the calculation than without radiation included. Thus, it may be said that even a small amount of radiative flux (5–6%) could produce a large error in the prediction, of the critical depressurization rate of the metalized propellant combustion.

Also, the calculation results have shown that dynamic extinction takes a little longer for combustion in the confined geometry than in the open geometry. The larger the burning area (A_b/A_t increases), the steeper is the depressurization rate B_p required for extinction. Finally, the higher P_f is, the larger the critical depressurization rate needs to be for dynamic extinction.

References

[1]Brewster, M. Q., and Parry, D. L., "Radiative Heat Feedback in Aluminized Solid Propellant Combustion," *Journal of Thermophysics*, Vol. 2, No. 2, 1988, pp. 123–130.

[2]Ciepluch, C. C., "Spontaneous Reignition of Previously Extinguished Solid Propellants," NASA TN-D-2167, 1964.

[3]Ciepluch, C. C., "Effect of Rapid Pressure Decay on Solid Propellant Combustion," *ARS Journal*, Vol. 31, 1961, pp. 1112–1122.

[4]Krier, H., T'ien, J. S., Sirignano, W. A., and Summerfield, M., "Nonsteady Burning Phenomena of Solid Propellants: Theory and Experiments," *AIAA Journal*, Vol. 6, No. 2, 1968, pp. 278–285.

[5]Kuo, K. K., Gore, J. P., and Summerfield, M., "Transient Burning of Solid Propellants," *Fundamentals of Solid-Propellant Combustion*, edited by K. K. Kuo and M. Summerfield, Vol. 90, Progress in Astronautics and Aeronautics, AIAA, New York, 1984, pp. 599–660.

[6]Merkle, C. L., Turk, S. L., and Summerfield, M., "Extinguishment of Solid Propellants by Depressurization: Effects of Propellant Parameters," AIAA Paper 69–176, Jan. 1969.

[7]De Luca, L., "Theory of Nonsteady Burning and Combustion Stability of Solid Propellants by Flame Models," *Nonsteady Burning and Combustion Stability of Solid Propellants*, edited by L. De Luca, E. W. Price, and M. Summerfield, Vol. 143, Progress in Astronautics and Aeronautics, AIAA, Washington, DC, 1992, pp. 519–600.

[8]Galfetti, L., Turrini, F., and DeLuca, L., "Modeling of Transient Combustion in Solid Rocket Motors," *16th International Symposium on Space Technology and Science*, ISAS, Tokyo, 1988, pp. 217–227.

[9]Ishihara, A., Brewster, M. Q., Sheridan, T. A., and Krier, H., "The Influence of Radiative Heat Feedback on Burning Rate in Aluminized Propellants," *Combustion and Flame*, Vol. 84, Nos. 1–2, 1991, pp. 141–153.

[10]Tang, K. C., and Brewster, M. Q., "Numerical Analysis of Radiative Heat Transfer in an Aluminum Distributed Combustion Region," *Numerical Heat Transfer*, Pt. A, Vol. 22, 1992, pp. 323–342.

[11]Zebrowski, M. A., and Brewster, M. Q., "Theory of Unsteady Combustion of Solids: Investigation of Quasisteady Assumption," *Journal of Propulsion and Power*, Vol. 12, No. 3, 1996, pp. 564–573.

[12]Zenin, A. A., "Thermophysics of Stable Combustion Waves of Solid Propellants," *Nonsteady Burning and Combustion Stability of Solid Propellants*, edited by L. De Luca, E. W. Price, and M. Summerfield, Vol. 143, Progress in Astronautics and Aeronautics, AIAA, Washington, DC, 1992, pp. 197–231.

[13]Nickerson, G. R., Coats, D. E., Hermsen, R. W., and Lamberty, L. T., "A Computer Program for the Prediction of Solid Propellant Rocket Motor Performance," AFRPL TR-83-036, Sept. 1984.

[14]Melcher, J. C., Krier, H., and Burton, R. L., "Burning Aluminum Particles Inside a Laboratory–Scale Solid Rocket Motor," *Journal of Propulsion and Power*, Vol. 18, No. 3, 2002, pp. 631–640.

[15]Galfetti, L., Riva, G., and Bruno, C., "Numerical Computations of Solid-Propellant Nonsteady Burning in Open or Confined Volumes," *Nonsteady Burning and Combustion Stability of Solid Propellants*, edited by L. De Luca, E. W. Price, and M. Summerfield, Vol. 143, Progress in Astronautics and Aeronautics, AIAA, Washington, DC, 1992, pp. 643–718.

[16]Zanotti, C., Volpi, A., Bianchessi, M., and DeLuca, L., "Measuring Thermodynamic Properties of Burning Propellants,"*Nonsteady Burning and Combustion Stability of Solid Propellants*, edited by L. De Luca, E. W. Price, and M. Summerfield, Vol. 143, Progress in Astronautics and Aeronautics, AIAA, Washington, DC, 1992, pp. 145–196.